

## Article

# Effects of Mode of Preparation of Titanium Dioxide Nanotube Arrays on Their Photocatalytic Properties: Application to *p*-Nitroaniline Degradation

Nisreen Alshibeh Alwattar<sup>1</sup>, Florence Vacandio<sup>2</sup> , Laurent Vassalo<sup>1</sup>, Thierry Djenizian<sup>2</sup>, Bruno Coulomb<sup>1</sup>   
and Jean-Luc Boudenne<sup>1,\*</sup> 

<sup>1</sup> Laboratoire Chimie Environnement (LCE), CNRS, Aix-Marseille University, 13331 Marseille, France

<sup>2</sup> MADIREL, CNRS, Aix-Marseille University, 13397 Marseille, France

\* Correspondence: jean-luc.boudenne@univ-amu.fr; Tel.: +33-41-355-1031

**Abstract:** The aim of this study was to investigate the photoactivity of dioxide titanium (TiO<sub>2</sub>) nanotube films depending on different structure factors including pore size, tube length, tube wall thickness and crystallinity. Aqueous *p*-nitroaniline was used as a probe to assess the photocatalytic activity of titanium dioxide nanotube layers under UV irradiations. Self-organized titanium dioxide nanotube thin films were prepared by electrochemical anodization of titanium (Ti) foils and Ti thin films sputtered onto silicon (Si). The amorphous as-formed titanium nanotube layers were then annealed at different temperatures ranging from 450 to 900 °C in order to form crystalline phases. The structure and the morphology of the films were characterized by surface analysis techniques and scanning electron microscopy, respectively. The photocatalytic activity of the resulting TiO<sub>2</sub> thin films was evaluated by monitoring the UV degradation of *p*-nitroaniline by UV spectrophotometry and by determining nitrification yields of by ion chromatography. The highest photocatalytic activity was exhibited for titanium nanotubes annealed at 450 °C. The presence of rutile—obtained for an annealing temperature of 900 °C—appeared to reduce the photodegradation yield of *p*-nitroaniline. Finally, the TiO<sub>2</sub> nanotubes obtained from Ti foils revealed the most efficient photocatalytic properties.

**Keywords:** anodization; annealing; photocatalysis; mineralization



**Citation:** Alshibeh Alwattar, N.; Vacandio, F.; Vassalo, L.; Djenizian, T.; Coulomb, B.; Boudenne, J.-L. Effects of Mode of Preparation of Titanium Dioxide Nanotube Arrays on Their Photocatalytic Properties:

Application to *p*-Nitroaniline Degradation. *Micro* **2023**, *3*, 369–381. <https://doi.org/10.3390/micro3010025>

Academic Editor: Ewa Kowalska

Received: 8 January 2023

Revised: 28 February 2023

Accepted: 9 March 2023

Published: 22 March 2023



**Copyright:** © 2023 by the authors. Licensee MDPI, Basel, Switzerland. This article is an open access article distributed under the terms and conditions of the Creative Commons Attribution (CC BY) license (<https://creativecommons.org/licenses/by/4.0/>).

## 1. Introduction

The presence of organic pollutants in water is a recognized issue of significant concern as a wide variety of these contaminants has been found in environmental matrices resulting in severe environmental and health issues. One way to overcome these sanitary and environmental problems are to develop efficient treatment procedures for the destruction of organic contaminants [1].

*p*-nitroaniline (PNA) is an organic amine compound found in industrial wastewater effluents where it is either manufactured or used as an intermediate or precursor in azo dyes, antioxidants, paints, agrochemicals, fuel additives, corrosion inhibitors, pesticides, antiseptic agents, medicines for poultry, and pharmaceutical synthesis [2–4]. PNA has been enlisted as one of the priority pollutants in water worldwide due to many serious eco-environmental problems due to its toxicity, potential carcinogenic and mutagenic effects [5,6]. The presence of PNA in water, even at very low concentrations, is extremely harmful to aquatic life and human health. The presence of a nitro group in the aromatic ring renders it very persistent and resistant to chemical and biological oxidation degradations, while the anaerobic degradation produces nitroso and hydroxylamines compounds which are known to be carcinogenic [7,8].

Advanced oxidation processes (AOPs) have been widely studied and developed to reduce or eliminate micropollutants in waters [9,10]. These processes refer to the technologies able to generate in-situ powerful oxidants, mainly hydroxyl radicals, whether of

chemical, physical, photochemical, photocatalytic or electrochemical nature. As compared to conventional technologies (such as those commonly used in wastewater plants), they are considered as effective processes to degrade recalcitrant organic contaminants without generating secondary hazardous by-products in the effluent [11]. This is a specifically important benefit over competing technologies such as chlorine oxidation, during which a considerable amount of organochlorinated species can be formed [12].

In recent years, water treatment using semiconductors particles has attracted attention and, among oxide semiconductors,  $\text{TiO}_2$  is often preferred (to  $\text{ZnO}$  for example) for heterogeneous catalysis because it does not generate toxic by-products [13] and presents excellent chemical and biological inertness properties, with low costs, and high oxidizing power under ultraviolet (UV) light irradiation [14–16]. However, the main drawback of  $\text{TiO}_2$  is its relatively broad energy band (3.2 eV for anatase and 3.0 eV for rutile) leading to photocatalytic activities only under UV light (wavelengths < 390 nm) [17,18]. Many organic contaminants (i.e., aromatic hydrocarbons, chlorinated aromatics, surfactants, etc.) can be fully mineralized on the surface of  $\text{TiO}_2$  nanoparticles in the presence of UV [19]. Typically,  $\text{TiO}_2$  is therefore used in the form of high surface area nanoparticles (such as the commercially available P25<sup>TM</sup> from Degussa (Sigma-Aldrich, Darmstadt, Germany)). This allows direct contact with a large amount of the surrounding medium and thus excellent mass transfer. However, the use of suspended particles suffers from disadvantages such as the need for a filtration step and a high charge carrier recombination rate, the latter being responsible for limited photocatalytic performance. These problems may be overcome by depositing the catalyst on an electrically conducting support allowing control of the photocatalytic activity with an applied electrochemical potential [20].

$\text{TiO}_2$  nanotubes ( $\text{TiO}_2$  NTs) have been widely studied since their discovery in 1998 by Kasuga et al. [21] and have today many applications ranging from microelectronics to energy and biology [22–24].  $\text{TiO}_2$  NTs can be elaborated by a variety of methods including deposition onto a nanoporous alumina template, sol-gel transcription using organo-chelators as template, seeded-growth, and hydrothermal processes [25]. However, of the nanotube fabrication route, the architecture demonstrating the most remarkable properties is highly ordered nanotube arrays made by anodization of titanium in fluoride-based baths [26–28]. Due to their high chemical stability and high specific surface area,  $\text{TiO}_2$  nanotubes can act as photocatalysts for various organic compounds in aqueous media [29–31]. Hence, the size of  $\text{TiO}_2$  nanotubes can be precisely tailored by controlling the electrochemical conditions i.e., the potential applied, the anodization time, and the chemical composition of the electrolyte [32,33]. However, the dimensions of the nanotubes are such that space charge layer (and related electronic properties such as band gap) in the nanotubes promotes electron-hole pair separation, which can also improve pollutants photocatalytic degradation [9].

Titania can exist in three different crystalline phases: anatase, rutile and brookite. Anatase has attracted attention for its prominent photocatalytic activity. The rutile phase is thermodynamically stable at high temperatures. The anatase and rutile phases crystallize in a tetragonal structure while brookite crystallizes in an orthorhombic structure [34,35]. The photocatalytic efficiency of the anatase-type crystal structure is known to be more effective than other crystal structures [36,37]. Zhang et al. in 2014 explained this higher photocatalytic activity of anatase by its indirect band gap preventing direct transitions from the conduction band to the valence band and thus allowing a longer lifetime of photoexcited electrons and holes (brookite and rutile belonging to the direct band gap semiconductor group) [38].

In the present work, we report the fabrication of self-organized  $\text{TiO}_2$  nanotubes thin films at room temperature by electrochemical anodization in a solution of  $\text{H}_3\text{PO}_4$  1M,  $\text{NaOH}$  1M, and 0.5 wt% HF. Two types of substrates were anodized: Ti foils and Ti thin films sputtered on silicon. The structure, morphology, and chemical composition of the samples were studied by X-ray Diffraction (XRD), Scanning Electronic Microscopy (SEM), and Energy-Dispersive X-ray Spectroscopy (EDS). The influence of annealing on

the structure and the chemical composition of the titanium nanotubes were investigated and the efficiency of heterogeneous photocatalytic activity for achieving the degradation of PNA is discussed.

## 2. Results

### 2.1. SEM and XRD Studies

Figure 1 shows the morphology of the catalysts before (Figure 1a,e) and after annealing (Figure 1b–d,f–h) electrochemically grown for both substrates. Before anodization, samples exhibited a uniform and highly ordered nanotubes arrangement, suggesting that the nanotube formation was not influenced by the nature of the Ti substrate. The diameters of the TiO<sub>2</sub> nanotubes were around 80 nm for Ti/Si (Figure 1a) and 95 nm for Ti foil substrates (Figure 1e). The examination of the SEM cross-section in Figure 1a shows in both cases a thickness of the TiO<sub>2</sub> layer of about 0.8 μm.

Figure 1b,f show the morphology of the samples annealed at 450 °C (in air for 3 h). The tubes were well defined with no alteration. Nevertheless, the average pore size was around 100 nm, indicating an enlargement of pore size especially for TiO<sub>2</sub> on Ti/Si. From Figure 1c,g, it is also apparent that the tubes were perfectly preserved after a thermal treatment performed at 650 °C. The average diameter of the pores was about 100 nm for both samples as observed previously. However, the nanotubular structure collapsed when the samples were annealed at 900 °C (Figure 1d,h).

Results of EDX analysis are given in Table 1 for all samples. The chemical composition of as-formed titanium nanotube layers grown at room temperature was understoichiometric with an O/Ti ratio between 1.23 and 1.26. This result suggests the presence of oxygen vacancies in the structure, which is in agreement with works reported by Chen et al. in 2016 [25] and Lim et al. in 2018 [26]. But after annealing, the resulting chemical composition of the oxide revealed an excess of oxygen. Indeed, the results show that for TiO<sub>2</sub> samples obtained from Ti foils, the ratio O/Ti increases with increasing temperature. However, the stoichiometric composition was not reached.

**Table 1.** Chemical composition of TiO<sub>2</sub> samples before and after annealing (EDX analysis).

Annealing Temperature (°C)	Ti/Si					Ti Foils				
	% Ti Atomic	% O Atomic	Ratio O/Ti	Specific Area (nm <sup>2</sup> )	Pore i.d. (nm)	Ti % Atomic	%O Atomic	Ratio O/Ti	Specific Area (nm <sup>2</sup> )	Pore i.d. (nm)
No annealing	45.0	55.0	1.23	5.4 × 10 <sup>6</sup>	93	44.3	55.7	1.26	4.9 × 10 <sup>5</sup>	95
450	36.7	63.3	1.72	6.4 × 10 <sup>6</sup>	101	40.3	59.7	1.49	4.9 × 10 <sup>5</sup>	96
650	44.8	55.2	1.23	5.9 × 10 <sup>6</sup>	97	36.6	63.4	1.73	3.5 × 10 <sup>5</sup>	96
900	38.2	61.8	1.62	-	-	35.6	64.6	1.81	-	-

Figure 2a,b shows the XRD patterns of the samples established in a grazing angle mode before and after annealing. Before anodization, both titanium nanotube films were amorphous: no peak could be attributed to a TiO<sub>2</sub> crystallized phase. But one can identify for TiO<sub>2</sub>/Ti foils (Figure 2b) four peaks located at 2θ = 35.1°; 38.4°; 40.2° and 53° corresponding to the titanium substrate (JCPDS file N° 44-1294) under the TiO<sub>2</sub> nanotubes film. A small titanium peak located at 2θ = 35.1° in the case of the Ti/Si substrate was detected (Figure 2a). Compared to Ti foil, the weak intensity of the peak can be explained by a lower thickness of the sputtered titanium film. Both samples annealed at 450 °C and 650 °C exhibited peaks at 2θ = 25.3°, 38.6° and 48° characteristic of the anatase structure (JCPDS file N° 21-1272). However, patterns of samples annealed at 900 °C were quite different and a mixture of anatase/rutile was obtained from Ti/Si: 3 peaks of anatase at 2θ = 25.3°; 38.5° and 48° and 4 peaks of rutile at 2θ = 27.4°; 36°; 41.2°; 54.4°. Only the four peaks attributable to the rutile phase (JCPDS Card No. 21-1276) were present when the nanotubes were obtained from titanium foils.

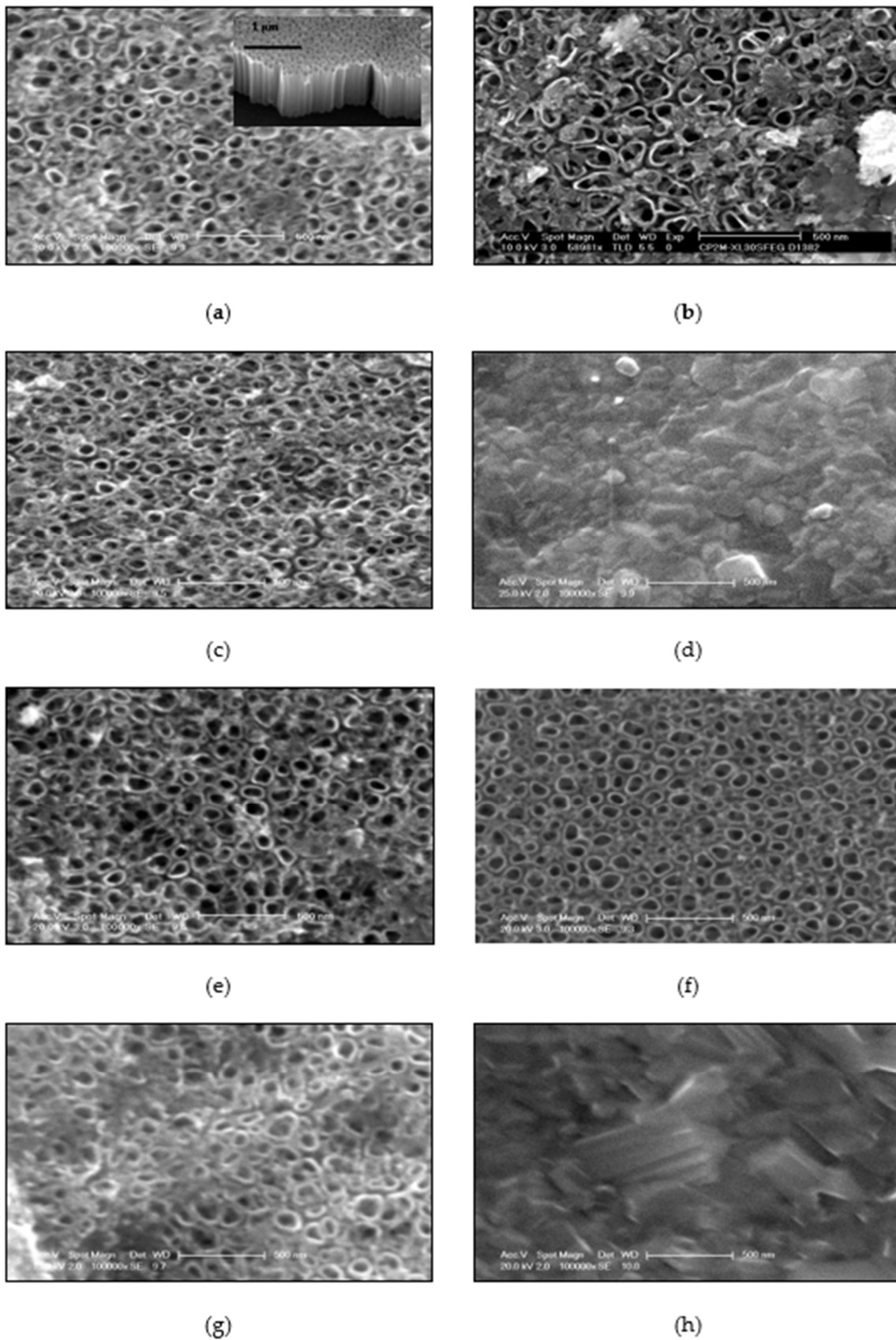


**Figure 1.** SEM images of  $\text{TiO}_2$  nanotubes obtained from Ti deposited on Si: (a) before annealing; (b) at 450 °C; (c) at 650 °C; (d) at 900 °C; and from Ti foils: (e) before annealing; (f) at 450 °C; (g) at 650 °C; (h) at 900 °C.

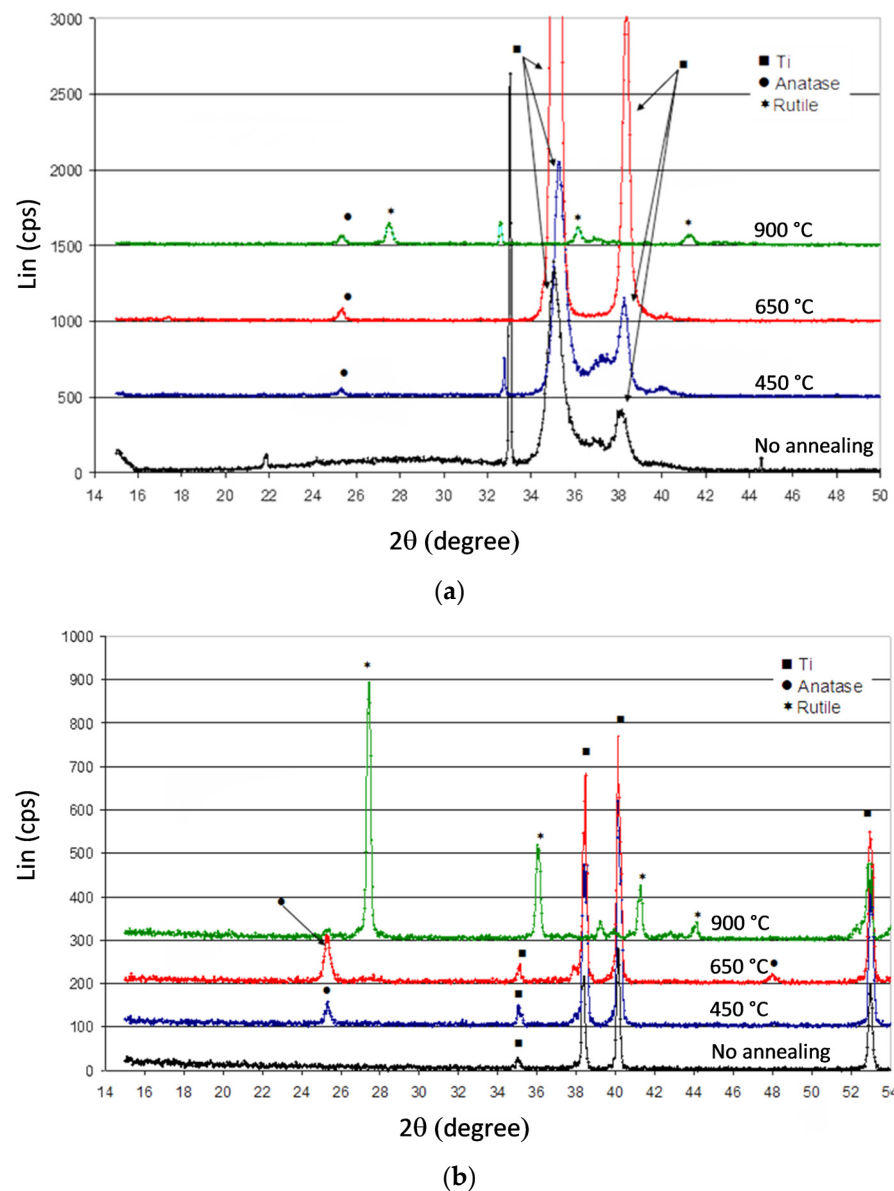


**Figure 2.** XRD Diagrams obtained in grazing incidence: (a) Ti deposited on Si; (b) Ti foil.

## 2.2. Photocatalytic Activity

### 2.2.1. Impact of the Annealing Temperature

The photocatalytic activity of the annealed titanium nanotubes was evaluated by monitoring degradation of PNA aqueous solutions under UV light irradiation during 150 min. Results are shown in Figure 3a,b respectively for samples of Ti deposited on Si and Ti foils, both annealed at different temperatures. From these results, it can be seen that calcination temperatures have a great influence on the photocatalytic activity of  $\text{TiO}_2$  nanotubes.

Photocatalytic activity seems primarily related to crystalline structure of  $\text{TiO}_2$  nanotubes: samples with tubular structure and large porous surface area (Figure 1a,e) showed a weak photocatalytic activity due to amorphous phase structure (Figure 2a,b). The degradation of PNA without  $\text{TiO}_2$  or with unannealed  $\text{TiO}_2$  stopped at 25 min. In the absence of  $\text{TiO}_2$ , degradation reached a maximum of 82%. This degradation was due to the direct photolysis by UV light emitted by the lamp (PNA absorbs mainly at 382 nm and UV lamp used in these experiments emit mainly at 365 nm).

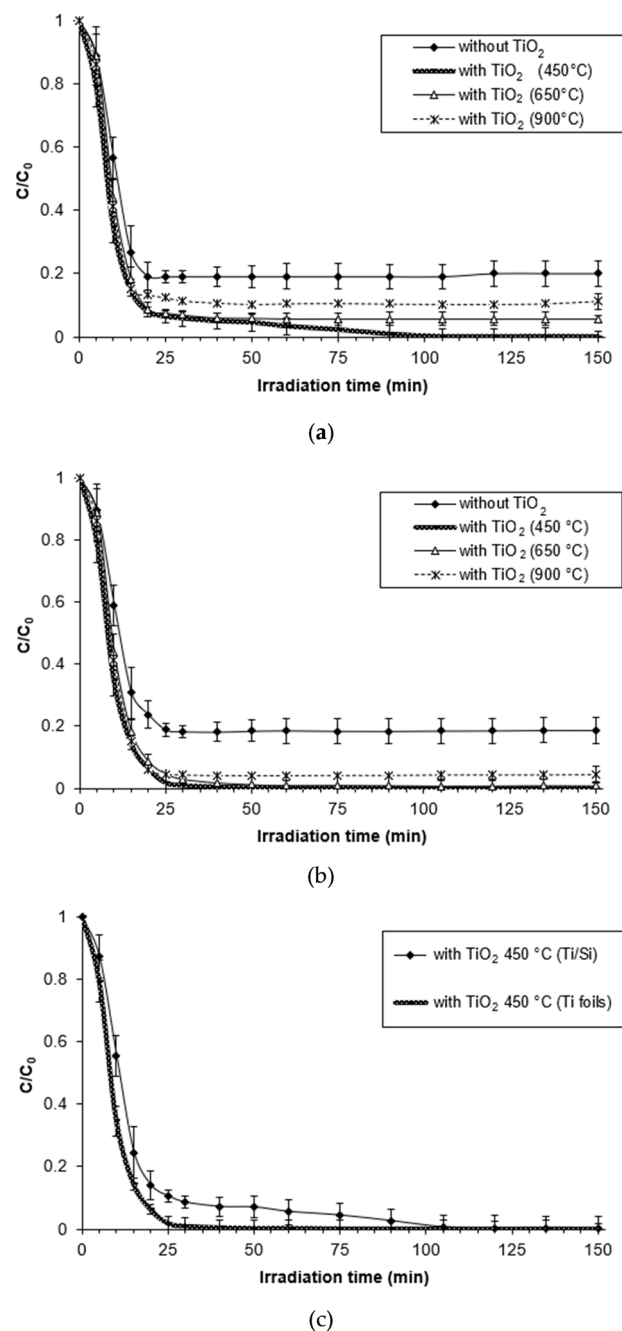


**Figure 3.** Photocatalytic activity of the TiO<sub>2</sub> samples annealed at various temperatures for the degradation of PNA in water: (a) with Ti deposited on Si substrate; (b) with Ti foil substrate; (c) Ti deposited on Si and Ti foils at 450 °C.

TiO<sub>2</sub> nanotubes annealed at 450 °C showed high photocatalytic activity with total degradation of PNA in 105 min and 30 min respectively for Ti/Si and Ti foils substrates (Figure 3c). These results could be due to the formation of the anatase phase with enhanced crystallinity and to the surface structure, as explained previously. These results are in good agreement with those reported by Viet and Tran in 2019 [29] who have shown that TiO<sub>2</sub> nanotube annealed at 400 °C and containing 100% anatase revealed the highest photocatalytic activity for the degradation of methylene blue. These results could also be explained by the increase in specific surface area and pore size of Ti/Si substrate annealed at 450 °C, while the annealing temperature seems to be less important in the surface change in the case of the Ti foils substrate (Table 1).

Photocatalytic activity of TiO<sub>2</sub> nanotubes decreases with increasing annealing temperature. However we can notice that this annealing temperature was more important for substrates based on Ti/Si than those based on Ti foil.

Finally, a lower photocatalytic activity was observed for TiO<sub>2</sub> nanotubes annealed at 900 °C due to the destruction of nanotubes arrays and the low photocatalytic activity of rutile phase formed [38].

We thus observed that the Ti foil substrates were more effective than Ti/Si substrates. This can be explained by the anodization on Ti foils which permitted to obtain more homogeneous formation of nanotubes on the whole surface of the blade than on Ti/Si substrates. The effect of annealing temperatures on PNA nitrification was also investigated (Figure 4). It was observed that nitrification performance was less than 12%. It would be necessary to carry out additional experiments to study the formation of intermediates (*p*-aminophenol, *p*-benzoquinone and hydroquinone that are well-known by-products of PNA degradation [39]) and radicals inhibiting compounds.

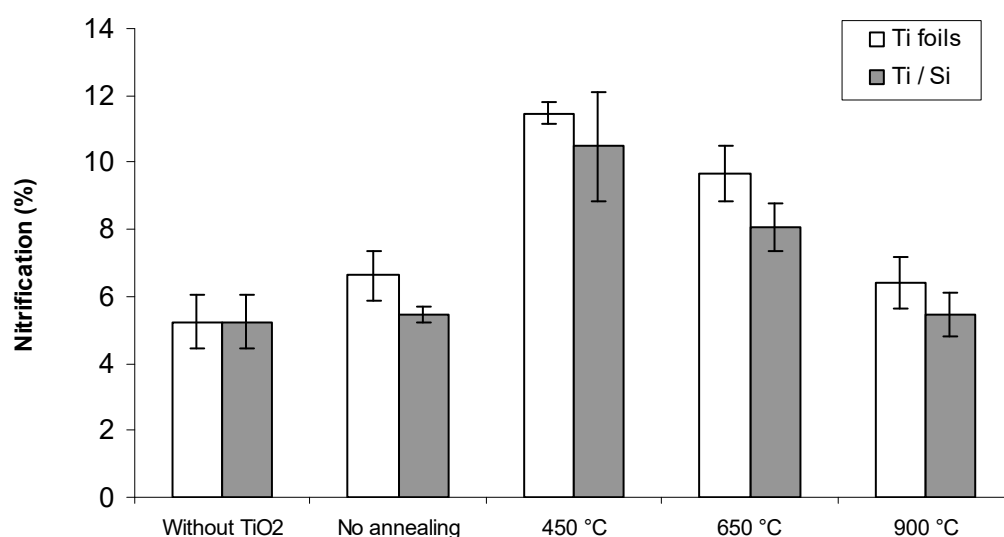


**Figure 4.** Nitrification of PNA using TiO<sub>2</sub> nanotubes prepared using two substrates: Ti deposited on Si and Ti foils, annealed at various temperatures.

However, we can observe that the most efficient nitrification was obtained with Ti foils substrates annealed at 450 °C.

#### 2.2.2. Distribution of End-Products vs. Nature of Substrate

TiO<sub>2</sub> nanotubes, deposited on Ti/Si and Ti foils substrates, and annealed at 450 °C have been specifically used to study the nature of end-products obtained after 40 min of UV irradiation of a 13.15 mg L<sup>-1</sup> PNA solution.

At the beginning of experiments carried out in triplicate, DOC, IC and TN were 6.28 mg C L<sup>-1</sup>, 0.54 mg C L<sup>-1</sup> and 2.67 mg N L<sup>-1</sup> (0.190 mmol N L<sup>-1</sup>) respectively. Figure 5a,b presents the variation of inorganic forms of nitrogen as a function of irradiation time. Results show firstly that the nitrogen organic part of PNA was fully recovered as inorganic forms (sum of NO<sub>3</sub><sup>-</sup>, NO<sub>2</sub><sup>-</sup> and NH<sub>4</sub><sup>+</sup> corresponds to the initial concentration of nitrogen). Moreover, nitrogen was mainly found as NH<sub>4</sub><sup>+</sup> at the end of photolysis; NO<sub>2</sub><sup>-</sup> and NO<sub>3</sub><sup>-</sup> were formed during the photodegradation process and seemed to be then reduced into NH<sub>4</sub><sup>+</sup>. Whatever the nature of substrate, distribution between the three forms of dissolved nitrogen appeared to be undifferentiated, even if amount of NH<sub>4</sub><sup>+</sup> produced with Ti foil substrate is higher than with Ti/Si substrate.

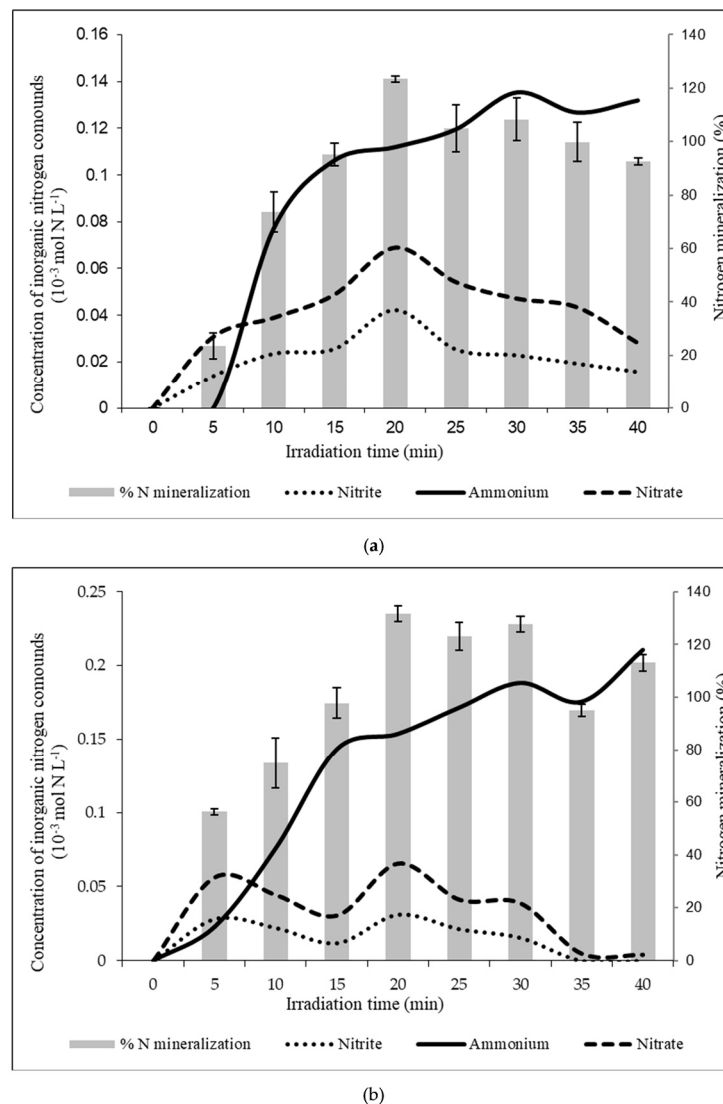
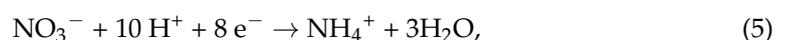
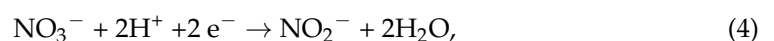


**Figure 5.** Evolution of inorganic forms of nitrogen (left axis) and nitrogen mineralization (right axis) during photocatalytic degradation of PNA carried out with: (a) Ti deposited on Si; (b) Ti foil.

Nitrate and nitrite reduction into ammonium is known when using wavelengths below 280 nm [40]. In such conditions, nitrates and nitrites are able to generate hydroxyl radicals that can contribute to the global photo-oxidation process. Moreover, when a catalyst as TiO<sub>2</sub> is used, Penpolcharoen et al. have shown in 2001 that nitrate could be reduced into ammonium as follows [41]:



As concerns the carbonaceous part of PNA, whatever the nature of substrate, decreases of DOC and TC of around 84% and 72% were observed respectively, with a parallel increase of IC of around 41% (Figure 6). Difference between DOC and IC at the end of the experiment could only be explained by the formation of CO<sub>2</sub> during the experiments.

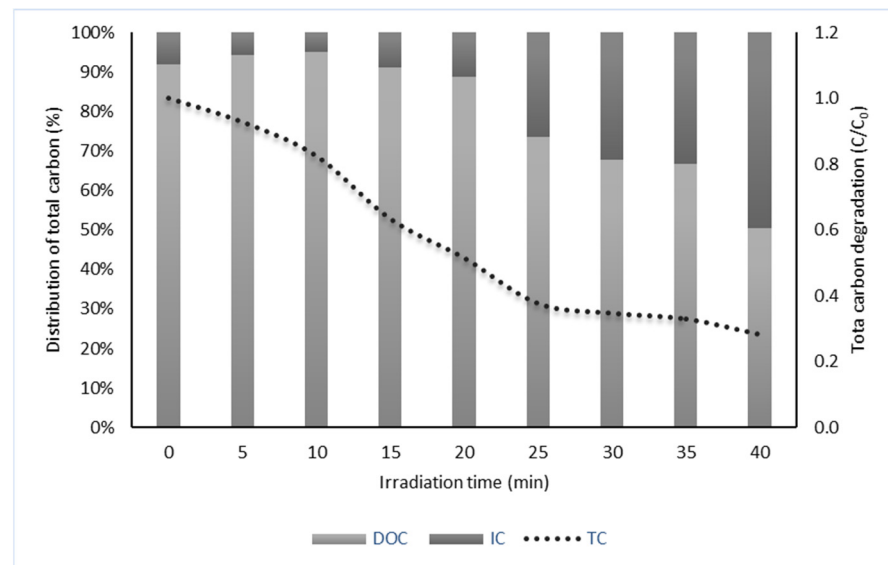


**Figure 6.** Distribution of inorganic and organic forms of carbon (**left axis**) and evolution of total carbon (**right axis**) during photocatalytic degradation of PNA.

This production of gaseous  $\text{CO}_2$  could be calculated according to DOC decrease, between the beginning and the end of the experiments, following:

$$\frac{(6.28 - 1.92) \text{ mg C L}^{-1}}{12 \left( \text{mg mmol}^{-1} \right)} = 0.408 \text{ mmol L CO}_2 \quad (6)$$

### 2.2.3. Degradation and Distribution of End-Products vs. pH

The photodegradation of PNA was studied with Ti/Si nanotubes as a function of pH, in a range varying between  $\text{pH} = 3.5$  and  $\text{pH} = 9.5$ . The results showed that the degradation kinetics is faster at basic pH. The yields obtained were 82%, 95% and 100%, respectively at  $\text{pH} = 3.5$ ,  $\text{pH} = 4.5$  and  $\text{pH} \geq 5.5$ , after 40 min of UV-irradiation. The degradation efficiency of PNA reaches more than 90% at pH above 5.5 after 20 min of irradiation against only 65% at  $\text{pH} = 3.5$ . This difference could be explained by the protonation of the  $-\text{NH}_2$  group of PNA into  $-\text{NH}_3^+$  in acidic medium, and thus the lower affinity of PNA for  $\text{TiO}_2$  which is also positively charged [39,42]. On the other hand, in basic medium, the generation of  $\text{OH}\bullet$  radicals is favored by the oxidation of  $\text{HO}^-$  ions adsorbed on the surface of the semiconductor, and the  $\text{HO}\bullet$  radicals thus photogenerated react with PNA, leading to its degradation [43].

Concerning the nitrogenous mineral forms obtained after UV irradiation as a function of pH, the increase of pH was found to drive the reaction towards a decrease of the production of  $\text{NH}_4^+$  ions, without however increasing the contents of nitrite and nitrate ions which seem to remain consumed during the photodegradation reactions. At basic pH ( $\text{pH} > 8$ ), the formation of nitrogen gas was thus supposed to be obtained.

Looking at the fate of the carbonaceous forms of PNA as a function of pH, the results showed that increasing pH resulted in no gaseous  $\text{CO}_2$  being generated and 84% of the initial PNA being converted to bicarbonates/carbonates.

## 3. Materials and Methods

### 3.1. Electrochemical Fabrication of Self-Organized Titanium Nanotubes

Titanium nanotubes were prepared by anodization of two different titanium substrates: Ti foils (0.127 mm thickness, 99.7% purity from Sigma Aldrich (Darmstadt, Germany)) and Ti films deposited on *p*-type Si(100) wafers with a resistivity of  $10^{-10} \Omega \text{ cm}$  (Wafer World Inc., Palm Beach, FL, USA) by cathodic sputtering of a Ti target (99.5% purity; diameter of 5 cm)

using a D.C. triode system. Before being introduced into the sputtering chamber, the silicon substrates were cleaned by sonicating successively in acetone, isopropanol, methanol and 1% HF solution during 30 s to eliminate the contamination layer on the surface, rinsed with deionized water (DI) and dried in a nitrogen stream. Prior deposition the chamber pressure was  $10^{-7}$  Torr. The argon partial pressure was maintained at  $6 \times 10^{-4}$  Torr during deposition. Under these conditions, the deposition rate was 16 nm/min and a 1.2  $\mu\text{m}$  thick Ti film was obtained after 120 min. Before anodization, all substrates were degreased by sonicating in acetone, isopropanol, and methanol, rinsed with deionized water (DI), and dried in a nitrogen stream. The as-prepared samples were anodized at 20 V during 20 min in NaOH 1M,  $\text{H}_3\text{PO}_4$  1M, 0.5 wt% HF solution at room temperature (Galvanostat-Potentiostat PAR 2273, Princeton Applied Research, Oak Ridge, TN, USA) using a platinum foil as counter electrode. Samples were annealed at various temperatures: 450 °C, 650 °C or 900 °C for 3 h in air, at a heating rate of 10 °C/min (Nabertherm controller B180 rapid thermo-annealer).

### 3.2. Characterization of $\text{TiO}_2$ Nanotubes

The morphology of the samples was characterized by Scanning Electron Microscopy (SEM) using a Philips XL-30 SEM microscope equipped with an energy-dispersive X-ray spectrometer (EDS). The structures were determined by X-ray Diffraction (XRD) analysis using a Siemens D5000 diffractometer with the  $\text{Cu K}\alpha$  radiation ( $\lambda = 1.5406 \text{ \AA}$ ).

### 3.3. Photocatalytic Reaction Experiments

All experiments were performed in a glass cylindrical photoreactor (Figure 7), 6 cm in inner diameter and 13 cm in height, offering a working volume of 60 mL. Samples were irradiated with a 125 W polychromatic high pressure mercury lamp (Philips HPK UV lamp), placed in vertical position in the photoreactor inside a quartz tube. The  $\text{TiO}_2$  nanotubes supports consisted in 4  $\text{cm}^2$  blades, disposed vertically in the photoreactor between two glass stops. A peristaltic pump was used to circulate the sample through a Suprasil<sup>®</sup> quartz flow cell (1 cm pathlength) placed in the spectrophotometer.

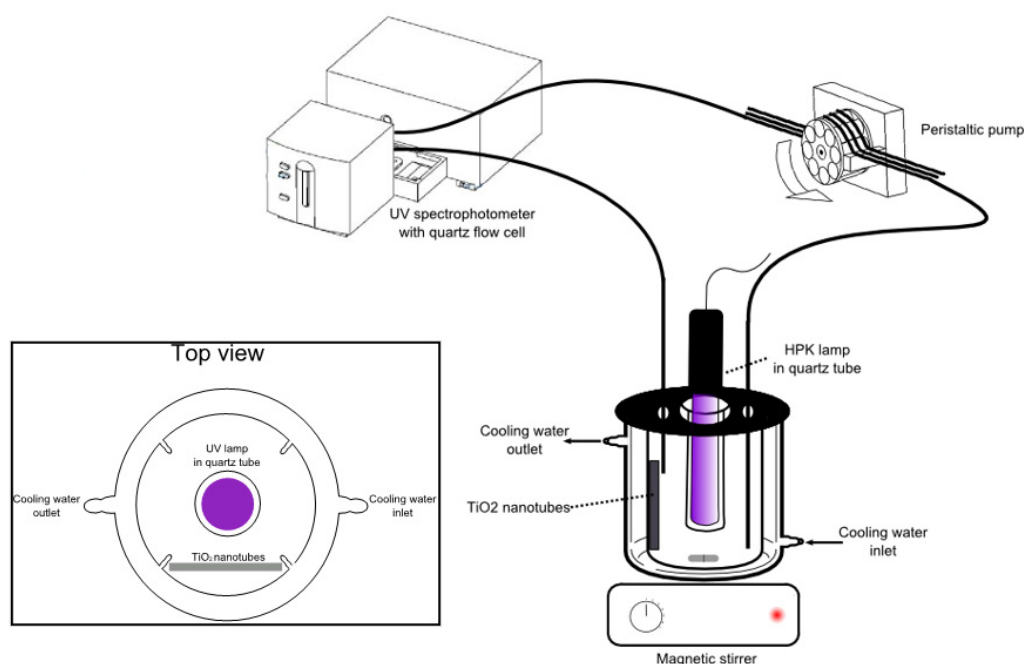


**Figure 7.** Experimental setup.

Experiments were carried out in triplicate with 10 mg L<sup>-1</sup> PNA solutions prepared from analytical grade *p*-nitroaniline purchased from Sigma-Aldrich using water from a Milli-Q water purification system (Millipore, Darmstadt, Germany), resistivity > 18 MΩcm).

### 3.4. Photocatalytic Reaction Experiments

The photocatalytic experiments were monitored by acquiring spectra in UV-visible range using a diode array spectrophotometer (Agilent 8453, Courtaboeuf, France). Degradation of PNA was followed by measuring the absorbance at 382 nm.

NO<sub>2</sub><sup>-</sup> and NO<sub>3</sub><sup>-</sup> levels were determined by Ion Chromatography using a Metrohm 761 SD compact IC, equipped with a 4 × 250 mm Metrosep column (Metrohm) as stationary phase, a mobile phase composed of NaHCO<sub>3</sub> (1.7 mM) + Na<sub>2</sub>CO<sub>3</sub> (1.8 mM) flowed at 1 mL.min<sup>-1</sup> and a conductimetric detector. NH<sub>4</sub><sup>+</sup> concentrations were followed by the commonly used indophenol blue method. Total Carbon (TC), Inorganic Carbon (IC) (and thus Dissolved Organic Carbon (DOC) by difference between TC and IC), and Total Nitrogen (TN) measurements were carried out using high temperature catalytic oxidation technique (Multi N/C 2100, Analytik Jena, Jena, Germany). The pretreated sample (50 µL) was injected into the furnace filled with a Pt preconditioned catalyst. The combustion was realized at 800 °C and the combustion products were carried by high purity oxygen (Linde Gas) allowing detection of CO<sub>2</sub> by non-dispersive infrared (NDIR) and detection of NO by chemiluminescence (CLD).

## 4. Conclusions

TiO<sub>2</sub> nanotubes were prepared by electrochemical anodization of two types of substrates: titanium foils and titanium thin films sputtered on silicon. The well-organized TiO<sub>2</sub> nanotubes grown from both substrates showing a diameter of about 100 nm are sub-stoichiometric and exhibit an amorphous structure. After annealing at 450 °C and 650 °C under air for 3 h, whatever the nature of the substrate, the nanotube morphology is perfectly preserved, and amorphous titanium is converted to the anatase phase. The O/Ti increases with increasing annealing temperature but remains below 2. At 900 °C, a mixture of anatase/rutile phases has been identified when TiO<sub>2</sub> nanotubes are elaborated from Ti/Si whereas the rutile phase is only present in the case of TiO<sub>2</sub> elaborated from Ti foils. However, the nanotubular structure is damaged after a thermal treatment performed at 900 °C.

Increasing the annealing temperature (up to 450 °C) promotes thus the crystallization in anatase phase and allows full elimination of *p*-nitroaniline within 30 min when Ti-based substrates are used.

**Author Contributions:** Conceptualization, F.V., T.D., B.C. and J.-L.B.; investigation, N.A.A. and L.V.; writing—original draft preparation, J.-L.B. and B.C.; supervision, F.V., T.D., B.C. and J.-L.B. All authors have read and agreed to the published version of the manuscript.

**Funding:** This research received no external funding.

**Institutional Review Board Statement:** Not applicable.

**Informed Consent Statement:** Not applicable.

**Data Availability Statement:** Not applicable.

**Conflicts of Interest:** The authors declare no conflict of interest.

## References

1. Balapure, A.; Ganesan, R. Anatase versus triphasic TiO<sub>2</sub>: Near-identical synthesis and comparative structure-sensitive photocatalytic degradation of methylene blue and 4-chlorophenol. *J. Colloid. Interface Sci.* **2021**, *581*, 205–217. [[CrossRef](#)] [[PubMed](#)]
2. Rajabizadeh, K.; Yazdanpanah, G.; Dowlatshahi, S.; Malakootian, M. Photooxidation process efficiency (UV/O<sub>3</sub>) for *p*-nitroaniline removal from aqueous solutions. *Ozone Sci. Eng.* **2020**, *42*, 420–427. [[CrossRef](#)]
3. Feng, G.Y.; Zhu, M.L.; Liu, L.; Li, C.B. A quantitative one-pot synthesis method for industrial azo pigments with recyclable wastewater. *Green Chem.* **2019**, *21*, 1769–1776. [[CrossRef](#)]

4. Lebkowska, M.; Rutkowska-Narozniak, A.; Pajor, E.; Tabernacka, A.; Zaleska-Radziwill, M. Impact of a static magnetic field on biodegradation of wastewater compounds and bacteria recombination. *Environ. Sci. Pollut. Res.* **2018**, *25*, 22571–22583. [[CrossRef](#)] [[PubMed](#)]
5. Gu, Y.L.; Wang, Y.Q.; Zhang, H.M. Study on the interactions between toxic nitroanilines and lysozyme by spectroscopic approaches and molecular modeling. *Spectrochim. Acta A* **2018**, *202*, 260–268. [[CrossRef](#)]
6. Silambarasana, S.; Vangnai, A.S. Biodegradation of 4-nitroaniline by plant-growth promoting *Acinetobacter* sp. AVLB2 and toxicological analysis of its biodegradation metabolites. *J. Hazard. Mater.* **2016**, *302*, 426–436. [[CrossRef](#)]
7. Li, K.; Zheng, Z.; Feng, J.; Zhang, J.; Luo, X.; Zhao, G.; Huang, X. Adsorption of p-nitroaniline from aqueous solutions onto activated carbon fiber prepared from cotton stalk. *J. Hazard. Mater.* **2009**, *166*, 1180–1185. [[CrossRef](#)]
8. Khalid, A.; Arshad, M.; Crowley, D.E. Biodegradation potential of pure and mixed bacterial cultures for removal of 4-nitroaniline from textile dye wastewater. *Water. Res.* **2009**, *43*, 1110–1116. [[CrossRef](#)]
9. Gopinath, K.P.; Madhav, N.V.; Krishnan, A.; Malolan, R.; Rangarajan, G. Present applications of titanium dioxide for the photocatalytic removal of pollutants from water. A review. *J. Environ. Manag.* **2020**, *270*, 110906. [[CrossRef](#)]
10. Titchou, F.E.; Zazou, H.; Afanga, H.; El Gaayda, J.; Ait Akbour, R.; Nidheesh, P.V.; Hamdani, M. Removal of organic pollutants from wastewater by advanced oxidation processes and its combination with membrane processes. *Chem. Eng. Process. Process. Intensif.* **2021**, *169*, 108631. [[CrossRef](#)]
11. Domingues, E.; Fernandes, E.; Gomes, J.; Martins, R.C. Advanced oxidation processes perspective regarding swine wastewater treatment. *Sci. Total Environ.* **2021**, *776*, 145958. [[CrossRef](#)]
12. Dewil, R.; Mantzavinos, D.; Poullos, I.; Rodrigo, M.A. New perspectives for Advanced Oxidation Processes. *J. Environ. Manag.* **2017**, *195*, 93–99. [[CrossRef](#)] [[PubMed](#)]
13. Quivet, E.; Höhener, P.; Temime-Roussel, B.; Dron, J.; Revenko, G.; Verlande, M.; Lebaron, K.; Demelas, C.; Vassalo, L.; Boudenne, J.-L. Underestimation of Anthropogenic Bromoform Released into the Environment? *Environ. Sci. Technol.* **2022**, *56*, 1522–1533. [[CrossRef](#)] [[PubMed](#)]
14. Bracco, E.; Butler, M.; Carnelli, P.; Candal, R. TiO<sub>2</sub> and N-TiO<sub>2</sub>-photocatalytic degradation of salicylic acid in water: Characterization of transformation products by mass spectrometry. *Environ. Sci. Pollut. Res.* **2020**, *27*, 28469–28479. [[CrossRef](#)]
15. Choi, Y.; Lee, D.; Hong, S.; Khan, S.; Darya, B.; Lee, J.Y.; Chung, J.; Cho, S.H. Investigation of the synergistic effect of sonolysis and photocatalysis of titanium dioxide for organic dye degradation. *Catalysts* **2020**, *10*, 500. [[CrossRef](#)]
16. Beheshti, F.; Tehrani, R.M.A.; Khadir, A. Sulfamethoxazole removal by photocatalytic degradation utilizing TiO<sub>2</sub> and WO<sub>3</sub> nanoparticles as catalysts: Analysis of various operational parameters. *Int. J. Environ. Sci. Technol.* **2019**, *16*, 7987–7996. [[CrossRef](#)]
17. Yuan, X.; Kobylanski, M.P.; Cui, Z.; Li, J.; Beauvier, P.; Dragoe, D.; Colbeau-Justin, C.; Zaleska-Medynska, A.; Remita, H. Highly active composite TiO<sub>2</sub>-polypyrrole nanostructures for water and air depollution under visible light irradiation. *J. Environ. Chem. Eng.* **2020**, *8*, 104178. [[CrossRef](#)]
18. Fatima, R.; Afridi, M.N.; Kumar, V.; Lee, J.; Ali, I.; Kim, K.H.; Kim, J.O. Photocatalytic degradation performance of various types of modified TiO<sub>2</sub> against nitrophenols in aqueous systems. *J. Clean. Prod.* **2019**, *231*, 899–912. [[CrossRef](#)]
19. Al-Mamum, M.R.; Kader, S.; Islam, M.S.; Khan, M.Z.H. Photocatalytic activity improvement and application of UV-TiO<sub>2</sub> photocatalysis in textile wastewater treatment: A review. *J. Environ. Chem. Eng.* **2019**, *7*, 103248. [[CrossRef](#)]
20. Maldonado-Larios, L.; Mayen-Mondragon, R.; Martinez-Orozco, R.D.; Paramo-Garcia, U.; Gallardo-Rivas, N.V.; Garcia-Alamilla, R. Electrochemically-assisted fabrication of titanium-dioxide/polyaniline nanocomposite films for the electroremediation of congo red in aqueous effluents. *Synth. Met.* **2020**, *268*, 116464. [[CrossRef](#)]
21. Kazuga, T.; Hiramutsu, M.; Hoson, A.; Sekino, T.; Niihara, K. Formation of titanium oxide nanotube. *Langmuir* **1998**, *14*, 3160–3163. [[CrossRef](#)]
22. Fraoucene, H.; Hatem, D.; Vacandio, F.; Pasquinelli, M. TiO<sub>2</sub> nanotubes with nanograss structure: The effect of the anodizing voltage on the formation mechanism and structure properties. *J. Electron. Mater.* **2019**, *48*, 2046–2054. [[CrossRef](#)]
23. Salian, G.D.; Koo, B.M.; Lefevre, C.; Cottineau, T.; Lebouin, C.; Tesfaye, A.T.; Knauth, P.; Keller, V.; Djenizian, T. Niobium alloying of self-organized TiO<sub>2</sub> nanotubes as an anode for lithium-ion microbatteries. *Adv. Mater. Technol.* **2018**, *3*, 1700274. [[CrossRef](#)]
24. Sugiawati, V.A.; Vacandio, F.; Galeyeva, A.; Kurbatov, A.; Djenizian, T. Enhanced electrochemical performance of electropolymerized self-organized TiO<sub>2</sub> nanotubes fabricated by anodization of Ti grid. *Front. Phys.* **2019**, *7*, 179. [[CrossRef](#)]
25. Chen, Z.; Cong, M.; Hu, J.; Yang, Z.; Chen, Z. Preparation of functionalized TiO<sub>2</sub> nanotube arrays and their applications. *Sci. Adv. Mater.* **2016**, *8*, 1231–1241. [[CrossRef](#)]
26. Lim, Y.P.; Yeo, W.H. The microstructure and mechanical properties of titanium dioxide nanotubes synthesized in the fluoride-based electrolyte. *Metall. Mater. Eng.* **2018**, *24*, 83–92. [[CrossRef](#)]
27. Nishanti, S.T.; Iyyapushpam, S.; Sundarakannan, B.; Subramanian, E.; Padiyan, D.P. Significance of crystallinity on the photoelectrochemical and photocatalytic activity of TiO<sub>2</sub> nanotube arrays. *Appl. Surf. Sci.* **2014**, *313*, 449–454. [[CrossRef](#)]
28. Hazra, A.; Bhowmik, B.; Dutta, K.; Manjuladevi, V.; Gupta, R.K.; Chattopadhyay, P.P.; Bhattacharyya, P. Formation mechanism of anodically grown free-standing nanotube array under the influence of mixed electrolytes. *Sci. Adv. Mater.* **2014**, *6*, 714–719. [[CrossRef](#)]
29. Viet, P.V.; Tran, H.N. Adsorption and photocatalytic degradation of methylene blue by titanium dioxide nanotubes at different pH conditions. *Adv. Nat. Sci. Nanosci. Nanotechnol.* **2019**, *10*, 045011. [[CrossRef](#)]

30. Cho, K.; Lee, S.; Kim, H.; Kim, H.E.; Son, A.; Kim, E.J.; Li, M.K.; Qiang, Z.; Hong, S.W. Effects of reactive oxidants generation and capacitance on photoelectrochemical water disinfection with self-doped titanium dioxide nanotube arrays. *Appl. Catal. B* **2019**, *257*, 117910. [[CrossRef](#)]
31. Ye, Y.; Bruning, H.; Liu, W.; Rijnaarts, H.; Yntema, D. Effect of dissolved natural organic matter on the photocatalytic micropollutant removal performance of TiO<sub>2</sub> nanotube array. *J. Photochem. Photobiol. A* **2019**, *371*, 216–222. [[CrossRef](#)]
32. Haq, S.; Rehman, W.; Waseem, M.; Meynen, V.; Awan, S.U.; Khan, A.R.; Hussain, S.; Zain-Ul-Abdin; Din, S.U.; Hafeez, M.; et al. Effect of annealing temperature on structural phase transformations and band gap reduction for photocatalytic activity of mesopores TiO<sub>2</sub> nanocatalysts. *J. Inorg. Organomet. Polym.* **2021**, *31*, 1312–1322. [[CrossRef](#)]
33. Nasirian, M.; Lin, Y.P.; Bustillo-Lecompte, C.F.; Mehrvar, M. Enhancement of photocatalytic activity of titanium dioxide using non-metal doping methods under visible light: A review. *Int. J. Environ. Sci. Technol.* **2018**, *15*, 2009–2032. [[CrossRef](#)]
34. Molina-Reyes, J.; Romero-Moran, A.; Uribe-Vargas, H.; Lopez-Ruiz, B.; Sanchez-Salas, J.L.; Ortega, E.; Ponce, A.; Morales-Sanchez, A.; Lopez-Huerta, F.; Zuniga-Islas, C. Study on the photocatalytic activity of titanium dioxide nanostructures: Nanoparticles, nanotubes and ultra-thin films. *Catal. Today* **2020**, *341*, 2–12. [[CrossRef](#)]
35. Castrejon-Sanchez, V.H.; Lopez, R.; Ramon-Gonzalez, M.; Enriquez-Perez, A.; Camacho-Lopez, M.; Villa-Sanchez, G. Annealing control on the anatase/rutile ratio of nanostructured titanium dioxide obtained by sol-gel. *Crystals* **2019**, *9*, 22. [[CrossRef](#)]
36. Hurum, D.C.; Agrios, A.G.; Gray, K.A. Explaining the enhanced photocatalytic activity of Degussa P25 mixed-phase TiO<sub>2</sub> using EPR. *J. Phys. Chem. B* **2003**, *107*, 4545–4549. [[CrossRef](#)]
37. Valeeva, A.A.; Dorosheva, I.B.; Kozlova, E.A.; Kamalov, R.V.; Vokhmintsev, A.S.; Selishchev Saraev, A.A.; Gerasimov, E.Y.; Weinstein, I.A.; Rempel, A.A. Influence of calcination on photocatalytic properties of nonstoichiometric titanium dioxide nanotubes. *J. Alloys Compd.* **2019**, *796*, 293–299. [[CrossRef](#)]
38. Zhang, J.; Zhou, P.; Liu, J.; Yu, J. New understanding of the difference of photocatalytic activity among anatase, rutile and brookite TiO<sub>2</sub>. *Phys. Chem. Chem. Phys.* **2014**, *16*, 20382–20386. [[CrossRef](#)]
39. Gautam, S.; Kamble, S.P.; Sawant, S.B.; Pangarkar, V.G. Photocatalytic degradation of 4-nitroaniline using solar and artificial UV radiation. *Chem. Eng. J.* **2005**, *110*, 129–137. [[CrossRef](#)]
40. Mack, J.; Bolton, J.R. Photochemistry of nitrite and nitrate in aqueous solution. A review. *J. Photochem. Photobiol. A* **1999**, *128*, 1–13. [[CrossRef](#)]
41. Penpolcharoen, M.; Amal, R.; Brungs, M. Degradation of sucrose and nitrate over titania coated nano-hematite photocatalysts. *J. Nanopart. Res.* **2001**, *3*, 289–302. [[CrossRef](#)]
42. Silva, C.G.; Wang, W.; Faria, J.L. Photocatalytic and photochemical degradation of mono-, di- and tri-azo dyes in aqueous solution under UV irradiation. *J. Photochem. Photobiol. A* **2006**, *181*, 314–324. [[CrossRef](#)]
43. Sanchez, L.; Peral, J.; Domenech, X. Photocatalyzed destruction of aniline in UV-illuminated aqueous TiO<sub>2</sub> suspensions. *Electrochim. Acta* **1997**, *42*, 1877–1882. [[CrossRef](#)]

**Disclaimer/Publisher's Note:** The statements, opinions and data contained in all publications are solely those of the individual author(s) and contributor(s) and not of MDPI and/or the editor(s). MDPI and/or the editor(s) disclaim responsibility for any injury to people or property resulting from any ideas, methods, instructions or products referred to in the content.